Hybrid solar energy device for simultaneous electric power generation and molecular solar thermal energy storage

Joule

CellPress
OPEN ACCESS

Article

Hybrid solar energy device for simultaneous electric power generation and molecular solar thermal energy storage

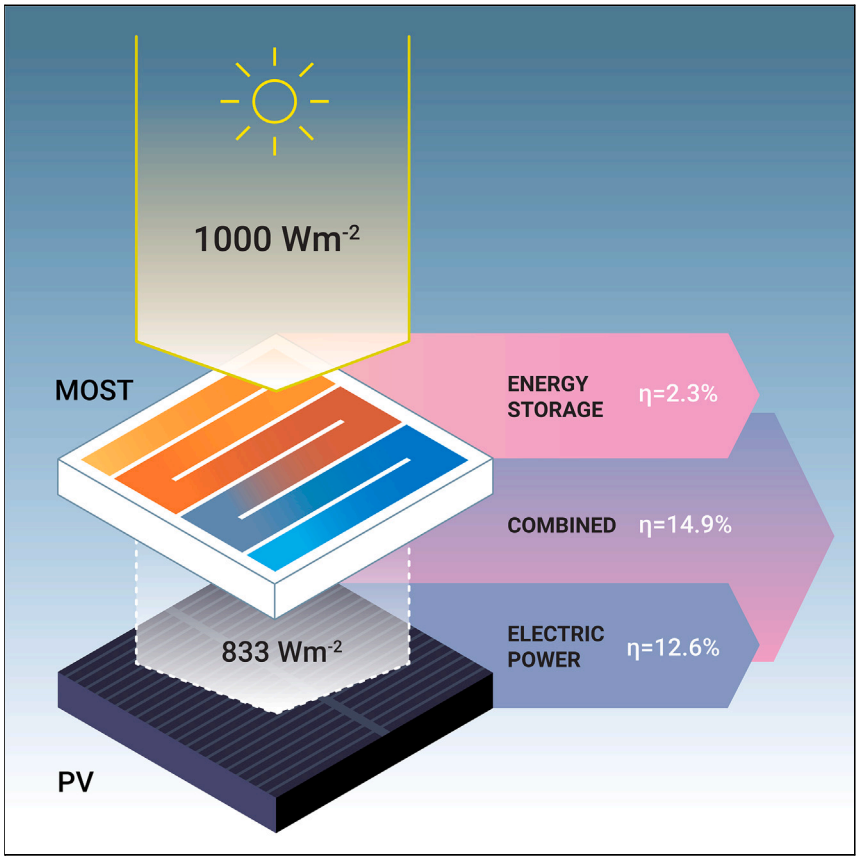

The efficiency of photovoltaic (PV) solar cells can be negatively impacted by the heat generated from solar irradiation. To mitigate this issue, a hybrid device has been developed, featuring a solar energy storage and cooling layer integrated with a silicon-based PV cell. This hybrid system demonstrated a solar utilization efficiency of 14.9%, indicating its potential to achieve even greater efficiencies in future advanced hybrid photovoltaic solar energy systems.

Zhihang Wang, Helen Hölzel, Lorette Fernandez, ..., Shima Ghasemi, Mariano Campoy-Quiles, Kasper Moth-Poulsen

kasper.moth-poulsen@chalmers.se

Highlights

A Si-based PV cell with a MOST flow cooling system shows improved solar efficiency

MOST solution can store UV and visible light, achieving 2.3% solar storage efficiency

MOST solution, as an optical filter, cools by 8°C and boosts PV cell efficiency by 0.2%

The hybrid device achieves 14.9% solar efficiency, surpassing individual devices

Wang et al., Joule 8, 2607–2622
September 18, 2024
Published by Elsevier Inc.
https://doi.org/10.1016/j.joule.2024.06.012

Joule

CellPress
OPEN ACCESS

Article

Hybrid solar energy device for simultaneous electric power generation and molecular solar thermal energy storage

Zhihang Wang,[1,2] Helen Hölzel,[2,3] Lorette Fernandez,[4] Adil S. Aslam,[2] Paulius Baronas,[4] Jessica Orrego-Hernández,[2] Shima Ghasemi,[2] Mariano Campoy-Quiles,[4] and Kasper Moth-Poulsen[2,3,4,5,6,*]

SUMMARY

The performance of photovoltaic (PV) solar cells can be adversely affected by the heat generated from solar irradiation. To address this issue, a hybrid device featuring a solar energy storage and cooling layer integrated with a silicon-based PV cell has been developed. This layer employs a molecular solar thermal (MOST) energy storage system to convert and store high-energy photons—typically underutilized by solar cells due to thermalization losses—into chemical energy. Simultaneously, it effectively cools the PV cell through both optical effects and thermal conductivity. Herein, it was demonstrated that up to 2.3% of solar energy could be stored as chemical energy. Additionally, the integration of the MOST system with the PV cell resulted in a notable decrease in the cell's surface temperature by approximately 8°C under standard solar irradiation conditions. The hybrid system demonstrated a solar utilization efficiency of 14.9%, underscoring its potential to achieve even greater efficiencies in forthcoming advanced hybrid PV solar energy systems.

INTRODUCTION

The world is currently undergoing a significant shift in its reliance on energy resources, transitioning away from fossil fuels and embracing renewable energy sources. In 2021, renewable primary energy experienced an impressive increase of 5.1 exajoules (EJ), reflecting an annual growth rate of 15%.[1] However, despite this progress, fossil fuels still account for 82% of the global energy mix, as revealed by the Statistical Review of World Energy 2022.[1] Among the various renewable energy sources, solar energy stands out as the most abundant on Earth and plays a vital role in electricity generation. In the European Union (EU) specifically, photovoltaic (PV) electricity already contributed 5.5% to the gross electricity output in 2021, demonstrating the promising potential of solar energy as a viable solution to meet the region's energy demands.[2] However, challenges such as local weather patterns and seasonal variations hinder the full utilization of solar power generation. To accelerate the transition to renewable energy sources, combining solar power conversion with long-term energy storage solutions becomes crucial. In this regard, the International Energy Agency's Net Zero Emissions by 2050 Scenario underscores the critical need for a significant expansion in grid-scale battery storage capacity. The target is to augment this capacity to about 44 times its current level, achieving around 680 GW by 2030.[2] Similarly, the Long Duration Energy Storage Council aims to expand the capacity of innovative long-duration storage technologies to between 1.5 and

CONTEXT & SCALE

The global shift from fossil fuels to silicon-based solar cells brings new challenges due to intermittent solar output and fluctuating energy demand, emphasizing the need for effective energy storage. Two main issues are (1) PV systems' efficiency drops by 10%–25% due to heating, requiring more land area, and (2) current storage technologies, like batteries, rely on unsustainably sourced materials. This paper proposes a hybrid device combining a molecular solar thermal (MOST) energy storage system with PV cell. The MOST system, made of elements like carbon, hydrogen, oxygen, fluorine, and nitrogen, avoids the need for rare materials. It serves as an optical filter and cooling agent for the PV cell, improving solar energy utilization and addressing the limitations of conventional PV and storage technologies.

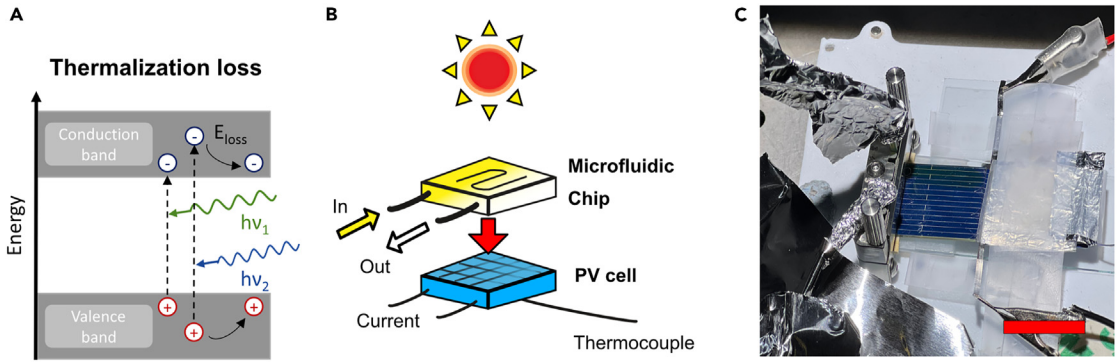

Figure 1. Hybrid device setup

(A) Schematic of the thermalization losses.

(B) Schematic of the hybrid device combining a microfluidic chip containing a molecular solar thermal (MOST) energy storage system and Si-based photovoltaic (PV) solar cells. The MOST fluidic chip was positioned on top of and in direct contact with the PV cell.

(C) Photo of the experimental setup under a solar simulator. The transparent MOST fluidic chip is positioned above the blue-colored Si-based PV cell shown in the middle of the photo (red scale bar, 2 cm).

2.5 TW by 2040. This expansion is intended to facilitate a cost-efficient, net-zero-emission energy system.[3] These projections clearly emphasize the essential role of cutting-edge energy storage technologies in enabling a seamless transition to a sustainable energy future.

Silicon (Si)-based PV systems have emerged as a dominant technology in solar energy conversion, with a global installed capacity exceeding 600 GW.[4] This remarkable growth can be attributed to several compelling advantages. Primarily, the abundant availability of Si on Earth, constituting 27.2 wt%, assures a steady and accessible supply for PV cell manufacturing, thereby minimizing dependence on limited resources.[5] Furthermore, the cost-effectiveness of Si-based PV modules has significantly increased over time, positioning solar energy as a strong competitor to traditional energy sources.[6] Its scalability facilitates the production of modules across a spectrum of sizes and power capacities, thereby offering versatility for numerous applications. Moreover, the established status of the Si-based PV industry, characterized by standardized manufacturing processes and extensive expertise, also greatly contributes to its widespread adoption and success. Notably, Si-based PV systems boast high efficiency in converting sunlight into electricity, with a recorded high of 27.6% under concentrated solar irradiation.[7] This impressive efficiency ensures the effective utilization of solar energy resources. Besides, Si-based PV modules offer exceptional reliability and longevity, with an average lifespan of around 30 years, making them a durable and enduring solution.[8] Lastly, but most importantly, recent research has proven that Si-based PV systems can contribute to environmental sustainability by generating clean and renewable energy, thereby reducing greenhouse gas emissions and mitigating the adverse impacts of fossil-fuel-based power generation.[9,10]

However, there are still challenges remaining that need to be addressed to maximize the efficiency of solar energy utilization. For instance, the absorption of solar radiation in connection with the band gap of the used semiconductor is crucial. When a short wavelength photon with energy greater than the band gap of Si is absorbed by a Si solar cell, the excess energy is converted into heat (Figure 1A). This is known as thermalization loss and is a substantial problem in all single-junction solar cells due to a considerable part of the solar spectrum comprising photons with energy

[1]Department of Materials Science and Metallurgy, University of Cambridge, 27 Charles Babbage Road, Cambridge CB3 0FS, UK

[2]Department of Chemistry and Chemical Engineering, Chalmers University of Technology, 41296 Gothenburg, Sweden

[3]Department of Chemical Engineering, Universitat Politècnica de Catalunya, EEBE, Eduard Maristany 10-14, 08019 Barcelona, Spain

[4]The Institute of Materials Science of Barcelona, ICMAB-CSIC, Bellaterra, 08193 Barcelona, Spain

[5]Catalan Institution for Research & Advanced Studies, ICREA, Passeig Lluìs Companys 23, 08010 Barcelona, Spain

[6]Lead contact

*Correspondence: kasper.moth-poulsen@chalmers.se

https://doi.org/10.1016/j.joule.2024.06.012

exceeding the semiconductor band gap.[11] Moreover, in PV designs, the effective utilization of high-energy photons is diminished due to the recombination of majority carriers within the space-charge region.[12] On the other hand, solar cell efficiencies for crystalline Si-based and thin-film PV modules are measured according to the standard test conditions (STCs) for solar panels, which, among others, entail a temperature of 25°C.[13,14] However, semiconductor solar cell efficiency is known to decrease significantly with its surface temperature, meaning that the efficiency under actual operating conditions can be lower than nominal.[15,16] Furthermore, it is worth noting that elevated temperatures can adversely affect the lifespan of solar modules.[17–20] Consequently, by operating the modules at lower temperatures, their longevity can be extended, leading to enhanced sustainability of the technology. This enhancement can hence positively affect the energy return on investment (EROI), which is defined as the ratio of energy output to energy input required for the fabrication and maintenance of the solar cell.

Diverging from the traditional method of combining a thermal absorber layer with a PV cell,[21] this study presents a novel approach. For the first time, we aim to address multiple challenges in PV technology, including overheating and inefficient utilization of high-energy photons. Additionally, this new method introduces solar thermal chemical storage into the system, offering a multifaceted solution to enhance overall efficiency. The basic idea is to combine a so-called molecular solar thermal (MOST) energy storage system with a Si-based PV cell. The MOST system is placed on top of the PV cell (Figure 1B) and contains a solution of photoswitchable organic molecules flowing through a microfluidic chip that can store sunlight as chemical energy via a photoisomerization process.[22–26] This process involves high-energy blue and ultraviolet photons (typically <450 nm) to convert parent molecules into high-energy metastable photoisomers. The energy stored in the MOST photoisomers can then be used as a backup energy source, either as a source of heat[27] or for thermoelectric power generation.[28] The MOST molecule is transparent at wavelengths longer than ≈450 nm; therefore, the majority of relevant photons are still available for the Si-based PV device. Meanwhile, the MOST layer reduces the thermal heating of the PV cell by filtering high-energy photons and actively cooling the microfluidic chip (*vide infra*), which enhances solar energy to power conversion.

In theory, an optimized and ideally operating MOST system with a 1.89-eV S_1-S_0 band gap has a maximum solar energy storage efficiency of 10.6%.[29,30] Additionally, this system offers the capability to directly store solar energy, enabling the mitigation of fluctuations across daily, seasonal, or even longer durations. However, despite the investigation of various MOST systems and corresponding devices,[23,31–37] experimental results indicate that MOST devices are still far from being optimized. For instance, for daily energy storage on an industrial scale, significant amounts of catalysts are necessary, coupled with a daily need for the extensive chemical energy stored, especially for applications with heating purpose.[38] On the seasonal storage and longer time frames, a large amount of MOST molecules and solvent will be needed.[31] Earlier studies on hybrid architectures, such as those converting solar energy to chemical energy storage and solar water heating, have shown enhanced combined efficiencies. However, the solar thermal energy storage efficiency $\eta_{experiment}$ of the reported MOST systems were limited, ranging from only 0.5% to 1.1%.[34] In this work, a $\eta_{experiment}$ of up to 2.3% is achieved, which is, to the best of our knowledge, a new world record. This was accomplished using a norbornadiene derivative, showing good performance in various factors, including solar spectrum match, storage energy capacity ($\Delta H_{storage}$), and photoisomerization quantum yield (φ_{iso}). The setup was designed and built by placing a commercial

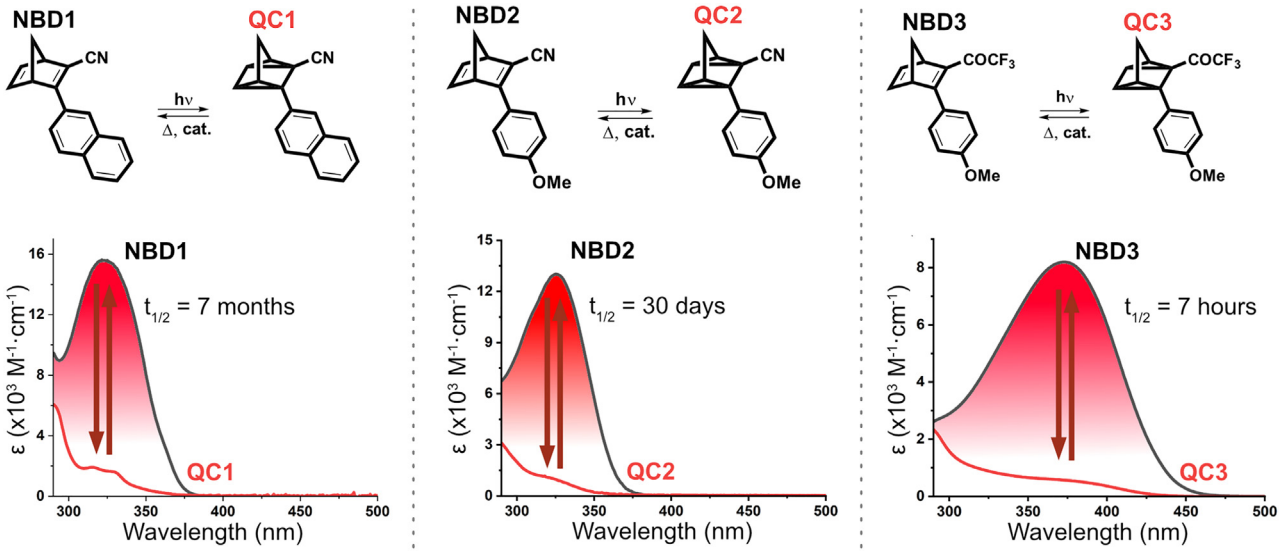

Figure 2. Molecular solar thermal energy storage systems and properties

Molecular structures, absorption profiles (ε is the molar absorption coefficient, all results were measured in toluene) of the parent norbornadiene derivative and their corresponding high-energy quadricyclane photoisomers used in this work. All listed half-life times were calculated at 25°C.

polycrystalline Si-based PV cell beneath the MOST system (Figures 1B and 1C). To ensure both effective cooling and optical filter (energy storage for non-heating temperature stabilization) effects from the MOST system, on one hand, the microfluidic chip containing the flowing MOST solution needs to be positioned in direct contact with the PV cell to maintain maximum thermal transfer. On the other hand, an appropriately high flow rate of the MOST solution can enhance the cooling of the PV cell while still maintaining a maximum $\eta_{experiment}$. Therefore, under such MOST flow conditions for temperature-stabilized operation, the PV cell is cooled down about 8°C, from 53°C to 45°C, with the help of the MOST fluid during solar irradiation, leading to a power conversion efficiency (PCE) boost of 12.6%. Together, the hybrid device operates at 14.9% solar utilization efficiency. Such presented results demonstrate the versatility of the concept and reveal important design parameters for future work on active MOST-based solar energy storage and PV cell cooling.

RESULTS AND DISCUSSION

MOST candidates

Three MOST systems based on the norbornadiene-quadricyclane (NBD-QC) molecular skeleton (Figure 2) were tested in this present setup as MOST fluid in a fused silica microfluidic chip (33.9 mm^3 with 100 μm optical pathlength) of the hybrid device. The rationales for the selection of the three NBD molecules—NBD1, NBD2, and NBD3— are their different photophysical properties, such as those related to the onset of absorption, thermal enthalpy barrier (ΔH_{therm} and ΔS_{therm}), energy storage half-life time ($t_{1/2}$), photoisomerization qumtum yield (φiso), and energy storage density ($\Delta H_{storage}$). The synthesis of the molecular systems was carried out according to the literature reports (Figures S1 and S2).[27,39–41] NBD1 has the largest thermal enthalpy barrier ΔH_{therm} of 169 kJ mol^{-1}, thus providing the longest half-life (8 months) among the three candidates (Table 1). NBD2 has a half-life time of 30 days and an onset of absorption of 380 nm. NBD3 exhibits the most red-shifted absorption spectrum with an onset of absorption at 457 nm; however, the $t_{1/2}$ of the corresponding QC-isomers (QC3) is only 7 h. Besides optical properties and $t_{1/2}$,

Table 1. Summary of photophysical properties (in toluene, λ_{cutoff} = 284 nm) of the three NBD candidates used in this work

Molecule	NBD onset (nm)	QC onset (nm)	ΔH_{therm} (kJ mol^{-1})	ΔS_{therm} (J mol^{-1} K^{-1})	$t_{1/2}$ at 25°C	φ_{iso} (%)	$\Delta H_{storage}$ (MJ mol^{-1})	η_{limit} (%)	$\eta_{experiment}$ (%)
NBD1	384	343	169	179	8 months	60	72	0.4	0.4
NBD2	380	345	104	−22	30 days	61	89	0.5	0.5
NBD3	457	402	72	−91	7 h	68	105	2.9	2.3

To calculate the thermal half-life $\left(t_{1/2} = \frac{ln\,(2)}{k}\right)$, the reaction rate constant k is determined using the Eyring equation $\left(k = \frac{k_B T}{h} e^{-\frac{\Delta H_{therm} - T\Delta S_{therm}}{RT}}\right)$, which involves both ΔH_{therm} and the entropy change (ΔS_{therm}).

both φ_{iso} and $\Delta H_{storage}$ are also key parameters. φ_{iso} signifies the probability of a conversion reaction occurring for each absorbed photon, whereas $\Delta H_{storage}$ crucially quantifies the solar energy storage capacity when the molecules are charged. As demonstrated in our previous work,[27] catalysts can be employed to release the stored energy as latent heat. The principle is that a higher energy density leads to a greater amount of heat being released. In this study, it reveals that φ_{iso} (approximately 60%–70%) and $\Delta H_{storage}$ (72–105 MJ mol^{-1}) are comparably similar across the three compounds under investigation, as detailed in Table 1. Based on a simulation framework that takes all the aforementioned factors into account, the maximal energy storage efficiency of the systems can be estimated. NBD1 and NBD2 can theoretically reach a maximum energy storage efficiency (η_{limit}, calculated by Equation 1 in experimental procedures section) of 0.4% and 0.5%,[27] respectively. Remarkably, the molecule NBD3, which exhibits the most red-shifted absorption and a φ_{iso} of 68%, has a theoretical maximum solar energy storage efficiency of 2.9%.[41]

PV solar cell characterization

For the hybrid device demonstration, a commercial polycrystalline Si-based PV cell was used. In order to evaluate how heat affects the performance of the PV cell (e.g., power generation efficiency), the PV device was characterized under irradiation from a class AAA solar simulator at different device temperatures, ranging from 8°C to 80°C. The temperature was varied using a custom-build holder that contains Peltier modules for cooling and heating.[42] The voltage-current curves were measured at different temperatures and the results indicate a linear correlation between the PCE and the temperature (Figure S3). This is the result of a strongly reduced open-circuit voltage with temperature arising from increased reverse saturation currents, which cannot be compensated by the slight increase in photocurrent related to a slightly broader absorption.[43] Such a phenomenon occurs in almost all PV technologies due to its fundamental origin.[44–46] Experimentally, the commercial PV cell was measured to lose around 25% of its PCE when heated from 8°C to 80°C.

Indoor demonstration

To demonstrate the hybrid concept, a series of experiments was performed with the molecules NBD1–3. First, investigations into the impact of flow rate on cooling efficiency were conducted using two solvents: toluene and water. It was found that the cooling effect of toluene closely parallels that of water, exhibiting a minimal difference of approximately 1°C in cooling performance at each tested flow rate. The optimal cooling effect with toluene occurs at the shortest residence time, achieved at a flow rate of 4 mL h^{-1}, as depicted in Figure S4. Furthermore, toluene's effectiveness in dissolving NBD derivatives positions it as a viable option for a heat transport solvent. Hence, solutions of the NBD1–3 molecules were prepared at a concentration of 0.1 M in toluene. The chosen high concentration of 0.1 M in our experiments

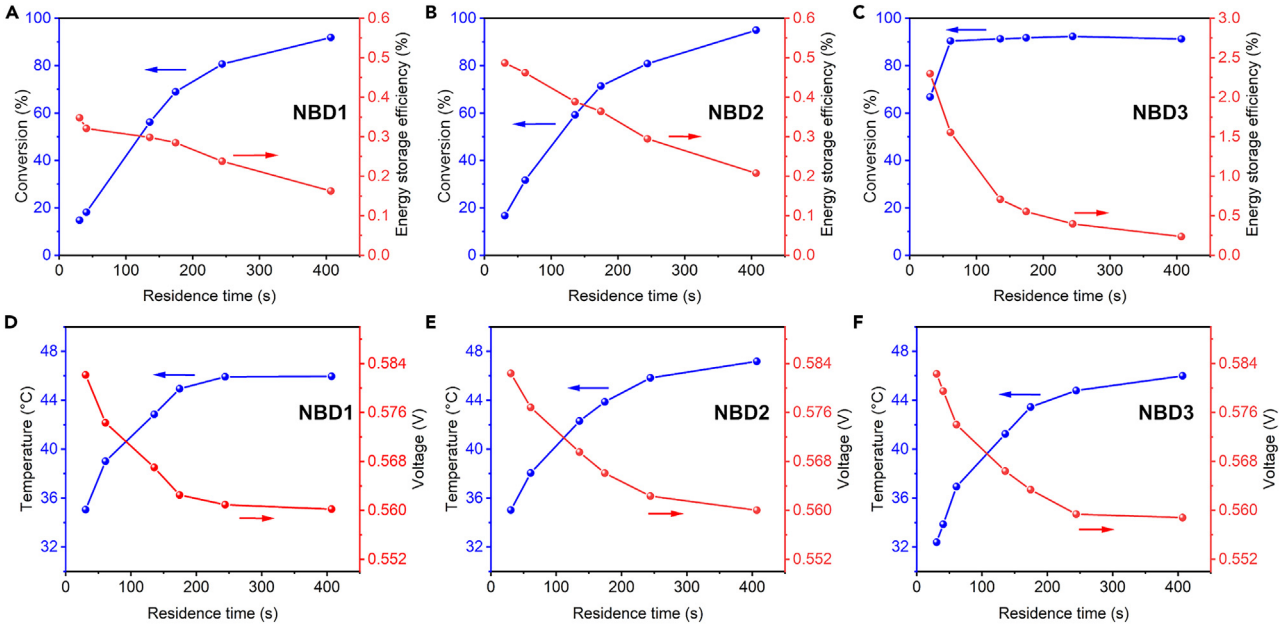

Figure 3. Performance data for the hybrid system

(A–C) Conversion percentage and energy storage efficiency over different residence times for NBD1–3 during indoor experiment testing.

(D–F) Surface temperature of the PV cell and open-circuit voltage generated over different residence times for NBD1–3 during indoor experiment testing (Table S1).

was determined by a meticulous balance between the solubility of the substances and the optical path length of the device. This concentration was also crucial for ensuring consistency in parallel comparisons with both the current work and previous studies.[28,34] A higher concentration of the MOST solution is also expected to provide additional optical filter effect from incoming UV sunlight, thereby enhancing the non-heating, temperature-stabilizing effect on the underlying PV cell. Following this, the NBD1–3 in toluene solutions were individually pumped through the microfluidic chip at different flow speeds. By varying the flow rate, and thereby the residence time, the MOST conversion percentage, as well as the energy storage efficiency, was determined.

As a result, the higher the flow rate of the MOST solution, the greater the energy storage efficiency achieved. Consequently, observations revealed that, with a high flow rate of 4 mL h^{-1} (residence time 31 s inside the chip; Figures 3A–3C), NBD1 and NBD2 can reach a maximum energy storage efficiency $\eta_{experiment}$ close to the theoretical estimate η_{limit} of 0.4% and 0.5%, with a conversion percentage of 15% and 17%, respectively (calculated with Equation 2 in experimental procedures section; Figure S5; Table S1). By increasing the solution residence time, nearly full conversion can be accomplished for NBD1 (92%) and NBD2 (95%). Theoretically, a red-shifted absorption spectrum (short excitation band gap) and a high φ_{iso} result in a higher energy-conversion percentage. Hence, for NBD3, with its significantly red-shifted absorption feature (475 nm) and a high φ_{iso} of 68% (surpassing the previous record high $\eta_{experiment}$ of 1.1%,[34] with an absorption onset at 456 nm and φ_{iso} of only 28%), a conversion percentage of 67% can be achieved at a rapid flow speed of 4 mL h^{-1}. This also provides a solar thermal energy storage efficiency $\eta_{experiment}$ of 2.3%, close to the estimate η_{limit} of 2.9%, exhibiting a new record for solar thermal energy storage performance in a flow device. To be highlighted, an essential parameter for optimization is the φ_{iso}-related conversion percentage ($\alpha_{conversion}$ factor in

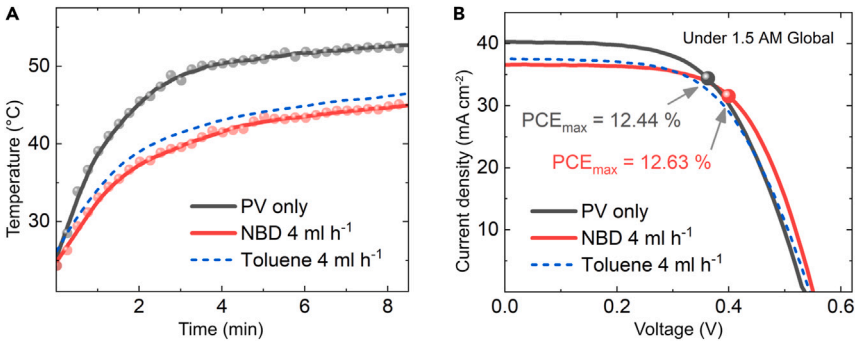

Figure 4. Thermal and photo-electric properties of the hybrid system with best-performing molecular system

(A) Surface temperature measurement of the PV cell. Black line shows the PV cell surface temperature without the MOST flow system on top. Blue dashed line shows the PV cell surface temperature with a 4 mL h^{-1} toluene flow system on top. Red line shows the PV cell surface temperature with a 4 mL h^{-1} NBD3 flow system on top.

(B) Photocurrent measurement of the PV cell with (red line), without the MOST flow system (black line), and toluene system (blue dashed line). A PCE_{max} up of 12.6% is measured with a 4 mL h^{-1} NBD3 flow system on top of the PV cell.

Equation 2 of the experimental procedures section). The influence of this percentage on efficiency is starkly revealed when comparing Figures 3A and 3B with Figure 3C, where an increase in the conversion percentage correlates with a significant drop in efficiency. Hence, high flow rate should be used to maintain a high-energy storage efficiency. Additionally, factors such as the spectral overlap between two isomers are very important. For example, a large spectral overlap between the parent molecule and its photoisomer allows for the accumulation of a higher number of converted molecules with extended residence time in the microfluidic chip. This accumulation competes with the NBDs' absorption, progressively diminishing the energy storage efficiency as the competition intensifies over time. This phenomenon can also be explained in the photoconversion process of NBD3, as investigated in our study. Such observations demonstrate that molecules with lesser spectral overlap, like NBD1 and NBD2, tend to show a more gradual reduction in energy storage efficiency as the residence time increases. This highlights the critical role of managing spectral overlap in optimizing MOST systems.

Additionally, it is noted that, with a higher flow rate, the surface temperature of the PV cell is reduced, thus resulting in a higher open-circuit voltage (V_{oc}, Figures 3D–3F; Table S1). The solutions of NBD1 and NBD2 lead to a low temperature of 35°C, and NBD3 lowers the temperature down to 31°C, with a V_{oc} of close to 0.6 V for all cases.

To further investigate the impact of surface heating from solar irradiation, NBD3—with the highest energy storage efficiency at high flow speed—was chosen to flow with 4 mL h^{-1} inside the microfluidic device.[47] When the device was exposed to a calibrated air mass 1.5 global (AM1.5G) solar spectrum, its surface temperature stabilized at approximately 45°C, as shown in Figure 4A. In comparison, a bare PV cell under the same conditions was stabilized at 53°C, indicating a significant temperature reduction of about 8°C with the device, subsequently resulting in a 0.2% increase in PV efficiency. As a control experiment, only toluene was circulated through the microfluidic chip at an identical flow rate. This led to the PV cell's surface temperature stabilizing at around 46.5°C, demonstrating a relatively weaker cooling effect with solvent-only cooling. The experimental data for toluene presented an intermediate cooling effect between the bare PV cell and the hybrid device incorporating

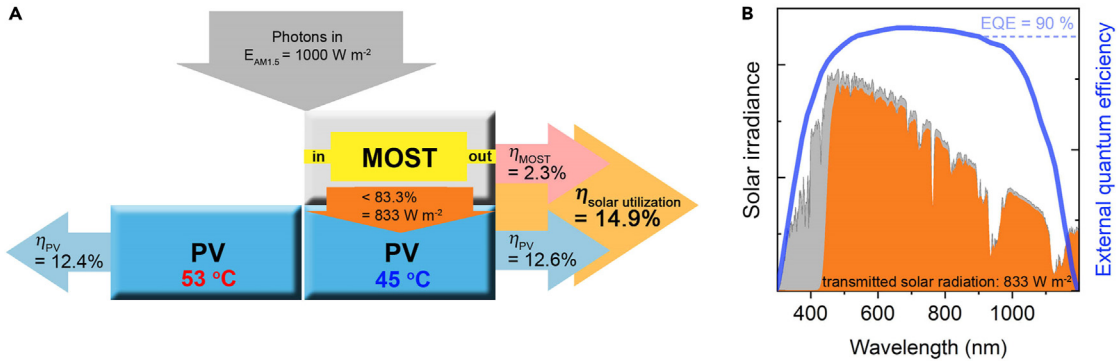

Figure 5. Detailed breakdown of energy losses

(A) Schematic presentation of the breakdown of photon management for both cases: PV cell alone (efficiency for PV cell alone: 12.4% of 100% incoming photons) operating at 53°C and PV cell with MOST system on top (efficiency: 12.6% for PV cell and MOST efficiency 2.3%, both of 100% incoming photons) operating at 45°C, leading to 14.9% solar utilization efficiency; loss of around 16.7% of incoming photons, transmittance of 83.3% of the photons after MOST system.

(B) Solar irradiation intensity and external quantum efficiency[51] vs. wavelength: AM1.5G solar radiation spectrum[52] (gray), transmitted solar radiation (orange, calculated by subtracting 4% due to normal reflection from fused silica surface of the chip and also subtracting the absorbed photons in the chip containing 0.1 M NBD3 in toluene), and external quantum efficiency (EQE, blue curve) reaching maximum 90%.

the MOST fluid. This finding is further supported by the fact that MOST fluid also serves as an optical filter, absorbing in the UV range as previously anticipated.

Despite photocurrent losses due to light reflection and UV absorption in the MOST device, a decrease in temperature also leads to reduced recombination rates, resulting in an increased V_{oc}. In the case of our Si-based PV cell, the V_{oc} is approximately 1.3 times greater at 8°C (0.63 V) than at 80°C (0.5 V), as detailed in Figure S3. Such an increase in V_{oc} resulting from cooling effectively offsets the optical losses in the PV system, which are attributable to the absorption properties of the MOST system. Hence, the PCE is finally increased by 0.2% (from 12.4% to 12.6% PCE; Figure 4B). These results show that the MOST solution does not negatively affect the performance of the PV cell because the cooling effect compensates for optical losses. The losses in photocurrent, in the case of only toluene and the MOST fluid compared with the PV cell alone, are rationalized by the design of the chip consisting of an interfering absorption. In future designs, this can be mitigated by reducing scattering from the channels, choosing a different glass material or an anti-reflective coating for the chip.

A comprehensive breakdown of all energy losses and efficiencies is illustrated in Figure 5A. The optical filtering and storage effect of NBD in toluene solution (accounting for 2.3% efficiency) and surface reflection losses in the MOST fluidic layer enable 83.3% of solar photons to reach the PV cell. This process optimally harvests UV and certain visible photons that are less efficient for the PV cell, as depicted in Figure 5B. Disregarding the optical effects of NBD3 in toluene solution, the MOST layer's cooling effect further improves the PV efficiency to 12.6%. Consequently, with an incoming solar irradiation of 1,000 W m^{-2}, the system achieves an efficiency output corresponding to a solar utilization rate of 14.9%.

To evaluate the MOST-PV hybrid device, it is useful to compare it with tandem PV cells, which are currently receiving considerable attention for their potential to exceed the efficiency limits of single-junction Si-based PV systems.[48] The mechanically stacked PV tandem solar cell comparable in geometry to a MOST-PV hybrid device would require a second semi-transparent, high-band-gap solar cell placed on top of a Si-based PV cell. Theoretically, a top UV-absorbing semiconductor cell

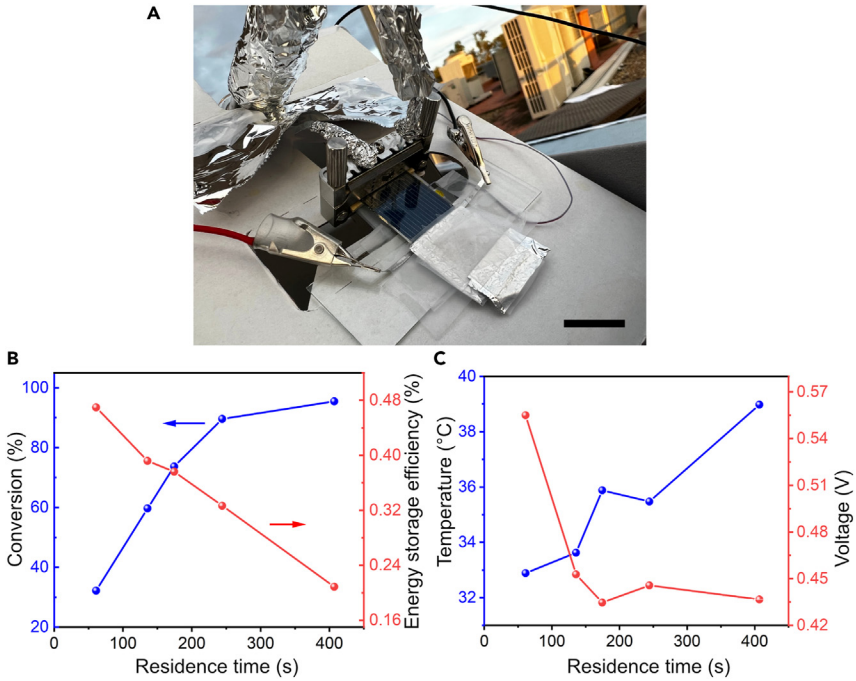

Figure 6. Real-life condition outdoor setup and performance

(A) Outdoor experimental setup figure (black scale bar, 2 cm).

(B) Conversion percentage and energy storage efficiency over residence time for outdoor demonstration.

(C) Surface temperature of the PV cell and generated voltage output over residence time for the outdoor demonstration (Table S2).

could have solar conversion efficiencies of up to 8.8% at an energy band gap of E_g = 2.7 eV,[49] but would require the integration and development of semi-transparent semiconductors and electrodes and efficient photon management. Realistically, current technologies of transparent UV-absorbing PV cells are reaching PCEs of 0.5% at E_g = 2.8 eV.[50] The detailed comparison of a MOST-PV hybrid device to analogous stacked tandem PV cell is presented in Figures S6 (theoretical values) and S7 (realistic values) in the supplemental information.

Outdoor demonstration

To ensure the concept's effectiveness in real-world scenarios and align with indoor experimental outcomes, the hybrid device was subjected to outdoor testing using NBD2. This choice was aimed at mitigating potential weather-related impacts, such as wind or cloud cover. NBD2 was selected due to its relatively prolonged $t_{1/2}$ of 30 days at 25°C, making it ideal for these conditions. The measurements were collected between 9 a.m. and 3 p.m. on 11th of November 2022 in Barcelona, Spain. During the experiment, the whole setup was manually oriented to face the sun (Figure 6A), and the measured solar power was close to 1 sun using a calibrated solar irradiation reference device.

In the outdoor test, the MOST system (NBD2) featured up to 97% conversion, with a residence time of 13.5 min (Figure 6B; Table S2). An energy storage efficiency of up to 0.5% was reached at a flow speed of 4 mL h^{-1}—nearly identical to the indoor experiments using simulated sunlight (0.5%). Related to the electrical potential generated from the PV cell (Figure 6C; Table S2), a maximum V_{oc} of 0.55 V at 36°C was obtained, slightly lower than the value obtained in the calibrated measurement

(Figure S3; Table S3; V_{oc} = 0.57 V at 39°C) that was measured using the solar simulator. This is very likely due to lower AM1.5G solar irradiation (less than 1 sun) during the measurement, caused by moving clouds and aperiodic cell cooling due to wind, meaning that the observed temperature and, thus, V_{oc} are greatly affected by the outdoor real-life conditions.

The combined efficiency of the hybrid system

Using the Shockley-Queisser (SQ) limit model for determining the efficiency limit for PV cells, the theoretical efficiencies of an optimal operating hybrid device on a simplified model was calculated using Equation 3 in the experimental procedures section. Based on previous simulations of the solar conversion efficiency for use in day-to-night energy storage (10.4%, 1.89 eV, S_0-S_1) or seasonal energy storage (12.4%, 1.81 eV, S_0-S_1),[29] as well as known SQ energy-conversion efficiency limits for a constant cell temperature (25°C),[53] the theoretical limits for the hybrid systems was then determined. For an average MOST efficiency in both cases of around 11% (1.85 eV), a temperature-controlled maximum efficiency of the single-junction PV cell of 32%, and with maximum PV efficiency of 26% at the same band gap as the MOST compound (1.85 eV), a combined efficiency of 16% (half of the PV single junction) of the hybrid can be reached within this model. In scenarios with a higher band gap of 2.4 eV, the losses can be further decreased to 7%, leading to an enhanced combined efficiency of 25% for the hybrid device (= 8% + 32% − 15%, as per Equation 3) at an operational temperature of 25°C. These figures represent conservative estimates, considering that the actual operational temperature of a cell in sunlight is typically much higher than 25°C, which consequently results in a notably lower PCE. Such theoretical estimation underscores the significant potential of a hybrid device that integrates an optimally designed MOST system.

Conclusions

PV technology is at the forefront of the global shift in energy production from fossil fuels to renewable sources. The efficiency and longevity of PV systems diminish as temperatures increase, resulting in significant reductions in energy output and cycling capability. Additionally, the growing importance of solar energy storage is underscored by the fluctuating nature of solar energy production and the variability in energy demand. Here, we introduce a possible PV-based hybrid technology that seeks to mitigate these challenges. This research introduces the pioneering combination of a PV solar cell with a MOST system, illustrating the feasibility of converting solar energy into chemical energy. The solar thermal energy storage efficiency $\eta_{experiment}$ of the MOST system has been determined to reach up to 2.3%, representing the highest recorded efficiency to date.[34] Additionally, the inclusion of the MOST system as a non-heating temperature stabilizer with optical filter effect can further enhance the efficiency of the PV cell. In a particular instance with Peltier cooling, it was observed that reducing the temperature of the PV cell from 51°C to 39°C can lead to an increase in PCE of 0.8% (value extracted from Figure S3). With the application of a MOST solution containing NBD molecules (NBD3), a reduction in the PV cell's surface temperature from 53°C to 45°C was achieved. This temperature decrease was associated with a modest 0.2% enhancement in PCE (from 12.4% to 12.6%), factoring in the optical losses encountered. Despite the potential for further optimization, this development is a significant stride toward a long-duration energy storage technology that complements PV systems. The combined MOST-PV system demonstrates the ability to produce more consistent power output across varying periods, from daily (NBD3 with $t_{1/2}$ = 7 h) to seasonal (NBD1 with $t_{1/2}$ = 7 months) cycles. Theoretically, the system can be configured to cycle different materials throughout the day to optimize efficiency. For instance, during periods of lower irradiance in the morning and afternoon, NBD1 or

NBD2 could be utilized within the microfluidic chip. In contrast, during peak sunlight hours, NBD3, known for its superior absorption and heat prevention capabilities, could be employed to more effectively collect and store solar energy. Finally, the potential of the hybrid system was further demonstrated using a simplified model based on the SQ limit, elaborated on in Equation 3 of the experimental procedures section. To be highlighted, a notable advantage of the MOST-PV hybrid system is its dual functionality, enabling simultaneous energy storage and electricity generation from solar power, thereby exemplifying an integrated approach to energy utilization.

To further assess the feasibility of the MOST fluidic device as a potential add-on technology for PV cells, which typically have a lifespan of more than 30 years,[8] a thorough consideration of several crucial factors of MOST is necessary. For instance, the cycling capacity of the photoswitch, as pointed out in the economic evaluation by Marangozls et al. in 1983 (with only 0.4% reported $\eta_{experiment}$, 2.3% in this work),[38] is critical in the development of MOST systems. Currently, MOST systems have been proven capable of over 1,000 cycles with minimal degradation.[54] In a real-world scenario with daily charging and discharging, a device operating continuously for months appears feasible. Future research should not only focus on small- and large-scale cycling tests with efficient catalysts but also on developing more red-shifted NBD candidates to enhance energy storage efficiency closer to the theoretical limit[29] of MOST systems. Furthermore, exploring techno-economic trade-offs in hybrid technology is vital, such as balancing the efficiency between the MOST system and PV cell (including band-gap matching) and considering thermal effects. Moreover, when integrating MOST systems with PV cells as an innovative heat-flow battery, the entire system should not show substantial capacity fade over time.[27,40] Hence, the life cycle assessment of a fully operational and optimized device should account for energy inputs, including those for fluid pumping. On the other hand, typical chemical storage implies the on-demand generation of electricity. However, in the case of MOST, this is not efficiently achievable unless through a thermoelectric effect.[28] This limitation delineates the scope of its application, underscoring the need for innovations in converting stored chemical energy into electricity more effectively. With these challenges and progress in mind, and the extensive implementation of PV technology worldwide, we can assume that a PV-MOST combination could be highly valued if a large-scale MOST device were developed.

EXPERIMENTAL PROCEDURES

Resource availability

Lead contact

Further information and requests for resources and procedures should be directed to the lead contact, Prof. Kasper Moth-Poulsen (kasper.moth-poulsen@chalmers.se).

Materials availability

This study did not generate new unique materials.

Data and code availability

All of the data supporting the findings are presented within the article and supplemental information. All other data are available from the lead contact upon reasonable request.

Materials

3-(naphthalen-2-yl)propiolonitrile was synthesized according to the synthetic pathway and according to a modified literature procedure (Figure S1A).[55] A 250-mL 3-neck round-bottom flask fitted with a dropping funnel and a reflux condenser was charged

with fresh $POCl_3$ (4.5 mL) under N_2 and cooled with an ice bath. Dimethylformamide (DMF, 9 mL) was then added dropwise under N_2. A solution of 2-acetonaphthone (2.05 g, 12.05 mol) in DMF (3 mL) was added dropwise to the reaction while cooling with the ice bath, followed by further addition of DMF (2 mL) under N_2. The reaction was removed from the ice bath and placed into an oil bath and heated at 60°C for 3 h. It was then cooled to room temperature. The reaction mixture was poured into an ice-chilled $NaHCO_3$. The residue was transferred to a separating funnel and mixed with dichloromethane until the phases separated. The organic layer was washed with water and brine, finally dried over Na_2SO_4, and concentrated *in vacuo*. The crude was used in the next step without purification.

Molecular iodine (2.11 g, 8.3 mol) was added to chloro-aldehyde (1.8 g, 8.3 mol) in 40 mL of dichloromethane in a round-bottom flask. The reaction was placed in an ice bath, followed by the addition of 20 mL of 25% aqueous NH_3 solution portion-wise over 15 min. The ice bath was removed and the solution was stirred at room temperature for 5 h. A saturated $Na_2S_2O_3$ solution (35 mL) was added to neutralize the iodine. The phases were separated in a separating funnel. Organic layers were dried over $MgSO_4$, filtered, and concentrated *in vacuo*. The crude was used in the next step without purification.

Tetrahydrofuran (THF, 32 mL) was added to chloro-nitrile residue, followed by the addition of NaOH solution (1.6 g in 6.6 mL) portion-wise over 5 min. The solution was stirred for 24 h. A saturated $NaHCO_3$ solution (35 mL) was added, and the mixture was stirred for 30 min. Once the phases were separated, the THF phase was separated in a separating funnel and concentrated *in vacuo*. The residue was taken up in CH_2Cl_2 and washed with water. The organic layers were dried over Na_2SO_4 and concentrated *in vacuo*. The residue was purified over automated flash column chromatography using gradient elution (Ethyl Acetate/ Hexane: 1/10 to 3/20) to give 3-(naphthalen-2-yl) propiolonitrile (1,250 g, 58%). Characterization data were consistent with the literature.[55]

3-(4-Methoxyphenyl)-2-propynenitrile was synthesized according to the synthetic pathway (Figure S1A) according to a modified literature procedure, and characterization data consistent with the literature.[55]

1,1,1-Trifluoro-4-(4-methoxyphenyl)but-3-yn-2-one) was synthesized according to a literature procedure, characterization data were consistent with the literature.[56]

All the NBDs in this study were prepared via the Diels-Alder reaction from acetylenes and cyclopentadiene using a conventional batch procedure or via combined cracking and Diels-Alder reaction with dicyclopentadiene using the previously published flow synthesis method (Figure S2).[39] Flow synthesis offers the possibility for upscaling when run continuously. This results in a higher production rate. NBD1 was prepared in a traditional batch synthesis[40] and the production rate was estimated to reach up to 0.11 g h^{-1}. Synthesis of NBD1: a solution of 4 (500 mg, 2.82 mmol), cyclopentadiene (559 mg, 8.47 mmol), and toluene (4 mL) was sealed in a microwave vial and heated at 110°C for 16 h. The mixture was cooled and purified over automated flash column chromatography using gradient elution (E.A./Hex. 3/20 to 1/5) to give NBD1 (470 mg, 68.5%) as a white solid. Characterization data were consistent with literature.[40] Synthesis of NBD2 and NBD3: in comparison, NBD2 and NBD3, which were prepared using the flow method,[39] could be prepared with a rate of up to 9.71 g h^{-1} to this point. Further, upscaling is currently being investigated to lay the foundation for and foster the development of larger-scale devices, as estimated above. Characterization data were consistent with the literature.[27,39]

Indoor and outdoor conversion experiments

The microfluidic chip used in this work was fabricated from fused silica (ConScience AB, Gothenburg, Sweden); the channel depth was 100 μm. The chip[47] has a total volume of 33.9 mm^3. All NBD solutions were delivered to such a microfluidic chip using a Kds 100 Legacy Single Syringe Infusion Pump. Based on the previous device simulation model,[57] it is reasonable to assume that the NBD flow was in a turbulent regime. This implies that there is no concentration gradient in the height and width directions of the flow field.

PV solar cell performance measurements

The polycrystalline solar cells used in this work were purchased from Shenzhen Yima Technology. The cell size is 26 * 52 * 3 mm, with a described maximum power (p_{max}) of 0.2 W, V_{oc} of 0.5 V, and a short circuit current (I_{sc}) of 0.4 A. Current and voltage of the solar cell was measured with a sourcemeter (Keithley 2450). Temperature changes of the solar cell were monitored by a Keysight Agilent 34972A LXI data acquisition unit. When doing the indoor and outdoor experiments, half of the solar cell was covered with aluminum foil (active area: 1.9 * 2.1 cm) to prevent unwanted exposure from solar irradiation. Raw data of PV temperature vs. time, PV photocurrent vs. volta presented in Figures 4A and 4B can be found in Tables S4 and S5.

The solar simulator used in this work was a AAA Solar Simulator conforming to the AM1.5G spectrum (SAN-EI Electric, XES-100S1). Irradiation from the solar simulator was calibrated to 1,000 W m^{-2} using an NREL-certified Si reference cell (Oriel Instruments, 91150V). The homogeneous illumination area was 100 * 100 mm.

Solar energy storage efficiency simulation details

To calculate the theoretical solar energy storage efficiency limit at a constant pressure in a given transparent fluidic device, Equation 1 can be used[27,31]:

$$\eta_{\text{limit}} = \frac{\int_0^{\lambda_{onset}} \frac{E_{AM\ 1.5G}(\lambda)\cdot(1\ -\ \mathrm{T}(c,\lambda,L))\cdot\varphi_{iso}\cdot\Delta H_{storage}}{h\nu\cdot N_A}\cdot d\lambda}{\dot{E}_{AM\ 1.5G}}\cdot 100\ \% \qquad \text{(Equation 1)}$$

Where $E_{AM\ 1.5G}(\lambda)$ is the power density with AM1.5G solar irradiance at a specific wavelength λ, T(c, λ, L) is the optical transmittance depending on the concentration, wavelength, and for a specific optical path length; φ_{iso} is the unitless photoisomerization quantum yield; $\Delta H_{storage}$ is the energy storage enthalpy of the used photoswitchable system; N_A is the Avogadro constant; and $\dot{E}_{AM\ 1.5G}$ is the total energy of the AM1.5G solar irradiation spectrum, per unit of time and area.

Experimental solar energy storage efficiency calculations

To calculate the experimental energy storage efficiency, Equation 2 needs to be considered[27,31,34]:

$$\eta_{experiment} = \frac{\dot{n}_{\text{parent}}\cdot\alpha_{conversion}\cdot\Delta H_{storage}}{S\cdot\dot{E}_{AM\ 1.5}}\cdot 100\ \% \qquad \text{(Equation 2)}$$

where $\dot{n}_{\text{parent}}$ is the flow speed of the parent molecule in mol s^{-1}, S corresponds to the effective irradiated area of the device in m^2, and $\alpha_{\text{conversion}}$ represents the conversion ratio from the parent NBD state to the corresponding photoisomer QC state.

Efficiency determination of the hybrid device relying on the SQ model

$$\eta_{hybrid(MOST,PV)} \le \eta_{MOST}\left(E_{gap}^{MOST}\right) + \eta_{PV}\left(E_{gap}^{PV}\right) - \eta_{PV}\left(E_{gap}^{MOST}\right) \qquad \text{(Equation 3)}$$

where E_{gap}^{MOST} is the energy gap of the MOST device and E_{gap}^{PV} is the energy gap of the PV single-junction device, and the equation is valid only if the MOST absorbs a significant fraction of the light below its gap.

SUPPLEMENTAL INFORMATION

Supplemental information can be found online at https://doi.org/10.1016/j.joule.2024.06.012.

ACKNOWLEDGMENTS

This work was supported by the European Research Council (no. 101002131), the Swedish Energy Agency, the Göran Gustafsson Foundation, the Swedish Research Council (project. 2020-00686), Swedish Research Council Formas, the European Research Council (ERC) under grant agreement CoG, PHOTHERM—101002131, the Catalan Institute of Advanced Studies (ICREA), and the European Union's Horizon 2020 Framework Programme under grant agreement no. 951801. The authors are very grateful to Dr. Pedro Ferreira for help on the indoor experiments test, Dr. Marti Gibert Roca for designing and manufacturing the holder with temperature control for PV measurements, and Miquel Casademont Viñas for introducing the solar simulator in the Institute of Materials Science of Barcelona. The Spanish Ministerio de Ciencia e Innovación (MICINN) is gratefully acknowledged for its support through grant no. CEX2023-001263-S in the framework of the Spanish Severo Ochoa Centre of Excellence program and the AEI/FEDER (UE) grant PID2021-128924OB-I00 (ISOSCELLES).

AUTHOR CONTRIBUTIONS

Conceptualization and methodology, Z.W. and K.M.-P.; experimental investigation, Z.W., L.F., and P.B.; molecular synthesis, H.H., A.S.A., and J.O.-H.; formal analysis, Z.W., P.B., M.C.-Q., and S.G.; writing – original draft, Z.W.; writing – review and editing, Z.W., H.H., L.F., A.S.A., P.B., M.C.-Q., and K.M.-P.; funding acquisition, K.M.-P.

DECLARATION OF INTERESTS

The authors declare no competing interests.

Received: August 29, 2023
Revised: January 19, 2024
Accepted: June 17, 2024
Published: July 15, 2024

REFERENCES

1. The British Petroleum Company p.l.c (2022). Key World Energy Statistics 2022. https://www.bp.com/content/dam/bp/business-sites/en/global/corporate/pdfs/energy-economics/statistical-review/bp-stats-review-2022-full-report.pdf.
2. IEA (2022). Grid-scale storage. https://www.iea.org/reports/grid-scale-storage.
3. McKinsey & Company (2021). Net-zero power: Long-duration energy storage for a renewable grid. https://www.mckinsey.com/capabilities/sustainability/our-insights/net-zero-power-long-duration-energy-storage-for-a-renewable-grid.
4. Victoria, M., Haegel, N., Peters, I.M., Sinton, R., Jäger-Waldau, A., del Cañizo, C., Breyer, C., Stocks, M., Blakers, A., Kaizuka, I., et al. (2021). Solar photovoltaics is ready to power a sustainable future. Joule *5*, 1041–1056. https://doi.org/10.1016/j.joule.2021.03.005.
5. Greenwood, N.N., and Earnshaw, A. (1997). Chemistry of the Elements, Second Edition (Buttterworth-Heinemann), pp. 328–366. https://doi.org/10.1016/B978-0-7506-3365-9.50015-8.
6. Guo, Y., and Xiang, Y. (2022). Cost–benefit analysis of photovoltaic-storage investment in integrated energy systems. Energy Rep. *8*, 66–71. https://doi.org/10.1016/j.egyr.2022.02.158.
7. The National Renewable Energy Laboratory (2021). Best solar cell efficiency chart. https://www.nrel.gov/pv/cell-efficiency.html.
8. Zhai, P., and Williams, E.D. (2010). Dynamic hybrid life cycle assessment of energy and carbon of multicrystalline silicon photovoltaic systems. Environ. Sci. Technol. *44*, 7950–7955. https://doi.org/10.1021/es1026695.
9. Dubey, S., Jadhav, N.Y., and Zakirova, B. (2013). Socio-economic and environmental impacts of silicon based photovoltaic (PV) technologies. Energy Procedia *33*, 322–334. https://doi.org/10.1016/j.egypro.2013.05.073.
10. Liang, H., and You, F. (2023). Reshoring silicon photovoltaics manufacturing contributes to decarbonization and climate change mitigation. Nat. Commun. *14*, 1274. https://doi.org/10.1038/s41467-023-36827-z.
11. Hirst, L.C., and Ekins-Daukes, N.J. (2011). Fundamental losses in solar cells. Prog.

Photovolt.: Res. Appl. *19*, 286–293. https://doi.org/10.1002/pip.1024.

12. Crane, M.J., Kroupa, D.M., and Gamelin, D.R. (2019). Detailed-balance analysis of Yb3. Energy Environ. Sci. *12*, 2486–2495. https://doi.org/10.1039/C9EE01493D.

13. Durisch, W., Tille, D., Wörz, A., and Plapp, W. (2000). Characterisation of photovoltaic generators. Appl. Energy *65*, 273–284. https://doi.org/10.1016/S0306-2619(99)00115-4.

14. Zhang, Y., Jia, X., Liu, S., Zhang, B., Lin, K., Zhang, J., and Conibeer, G. (2021). A review on thermalization mechanisms and prospect absorber materials for the hot carrier solar cells. Sol. Energy Mater. Sol. Cells *225*, 111073. https://doi.org/10.1016/j.solmat.2021.111073.

15. Dubey, S., Sarvaiya, J.N., and Seshadri, B. (2013). Temperature dependent photovoltaic (PV) efficiency and its effect on PV production in the world – a review. Energy Procedia *33*, 311–321. https://doi.org/10.1016/j.egypro.2013.05.072.

16. Mani, M., and Pillai, R. (2010). Impact of dust on solar photovoltaic (PV) performance: research status, challenges and recommendations. Renew. Sustain. Energy Rev. *14*, 3124–3131. https://doi.org/10.1016/j.rser.2010.07.065.

17. Pascual, J., Martinez-Moreno, F., García, M., Marcos, J., Marroyo, L., and Lorenzo, E. (2021). Long-term degradation rate of crystalline silicon PV modules at commercial PV plants: an 82-MWp assessment over 10 years. Prog. Photovolt.: Res. Appl. *29*, 1294–1302. https://doi.org/10.1002/pip.3456.

18. Park, N.C., Oh, W.W., and Kim, D.H. (2013). Effect of temperature and humidity on the degradation rate of multicrystalline silicon photovoltaic module. Int. J. Photoenergy *2013*, 1–9. https://doi.org/10.1155/2013/925280.

19. Ogbomo, O.O., Amalu, E.H., Ekere, N.N., and Olagbegi, P.O. (2018). Effect of operating temperature on degradation of solder joints in crystalline silicon photovoltaic modules for improved reliability in hot climates. Sol. Energy *170*, 682–693. https://doi.org/10.1016/j.solener.2018.06.007.

20. Rahman, T., Mansur, A.A., Hossain Lipu, M., Rahman, M.S., Ashique, R.H., Houran, M.A., Elavarasan, R.M., and Hossain, E. (2023). Investigation of degradation of solar photovoltaics: a review of aging factors, impacts, and future directions toward sustainable energy management. Energies *16*, 3706. https://doi.org/10.3390/en16093706.

21. Chen, G., Wang, N.E., Boriskina, V.S., McEnaney, K., Ghasemi, H., Yerci, S., Lenert, A., Yang, S., Miljkovic, N., Weinstein, A.L., and Bierman, D. (2014). Internally-heated thermal and externally-cool photovoltaic cascade solar energy system for full solar spectrum utilization. https://patents.google.com/patent/US20150053266A1/en.

22. Yoshida, Z.-i. (1985). New molecular energy storage systems. J. Photochem. *29*, 27–40. https://doi.org/10.1016/0047-2670(85)87059-3.

23. Wang, Z., Erhart, P., Li, T., Zhang, Z.-Y., Sampedro, D., Hu, Z., Wegner, H.A., Brummel, O., Libuda, J., Nielsen, M.B., and Moth-Poulsen, K. (2021). Storing energy with molecular photoisomers. Joule *5*, 3116–3136. https://doi.org/10.1016/j.joule.2021.11.001.

24. Dong, L., Feng, Y., Wang, L., and Feng, W. (2018). Azobenzene-based solar thermal fuels: design, properties, and applications. Chem. Soc. Rev. *47*, 7339–7368. https://doi.org/10.1039/C8CS00470F.

25. Qiu, Q., Shi, Y., and Han, G.G.D. (2021). Solar energy conversion and storage by photoswitchable organic materials in solution, liquid, solid, and changing phases. J. Mater. Chem. C *9*, 11444–11463. https://doi.org/10.1039/D1TC01472B.

26. Cai, F., Song, T., Yang, B., Lv, X., Zhang, L., and Yu, H. (2021). Enhancement of solar thermal fuel by microphase separation and nanoconfinement of a block copolymer. Chem. Mater. *33*, 9750–9759. https://doi.org/10.1021/acs.chemmater.1c03644.

27. Wang, Z., Roffey, A., Losantos, R., Lennartson, A., Jevric, M., Petersen, A.U., Quant, M., Dreos, A., Wen, X., Sampedro, D., et al. (2019). Macroscopic heat release in a molecular solar thermal energy storage system. Energy Environ. Sci. *12*, 187–193. https://doi.org/10.1039/C8EE01011K.

28. Wang, Z., Wu, Z., Hu, Z., Orrego-Hernández, J., Mu, E., Zhang, Z.-Y., Jevric, M., Liu, Y., Fu, X., Wang, F., et al. (2022). Chip-scale solar thermal electrical power generation. Cell Rep. Phys. Sci. *3*, 100789. https://doi.org/10.1016/j.xcrp.2022.100789.

29. Börjesson, K., Lennartson, A., and Moth-Poulsen, K. (2013). Efficiency limit of molecular solar thermal energy collecting devices. ACS Sustainable Chem. Eng. *1*, 585–590. https://doi.org/10.1021/sc300107z.

30. Wang, Z., Moïse, H., Cacciarini, M., Nielsen, M.B., Morikawa, M.-A., Kimizuka, N., and Moth-Poulsen, K. (2021). Liquid-based multijunction molecular solar thermal energy collection device. Adv. Sci. (Weinh) *8*, e2103060. https://doi.org/10.1002/advs.202103060.

31. Wang, Z., Hölzel, H., and Moth-Poulsen, K. (2022). Status and challenges for molecular solar thermal energy storage system based devices. Chem. Soc. Rev. *51*, 7313–7326. https://doi.org/10.1039/D1CS00890K.

32. Lennartson, A., Roffey, A., and Moth-Poulsen, K. (2015). Designing photoswitches for molecular solar thermal energy storage. Tetrahedron Lett. *56*, 1457–1465. https://doi.org/10.1016/j.tetlet.2015.01.187.

33. Orrego-Hernández, J., Dreos, A., and Moth-Poulsen, K. (2020). Engineering of norbornadiene/quadricyclane photoswitches for molecular solar thermal energy storage applications. Acc. Chem. Res. *53*, 1478–1487. https://doi.org/10.1021/acs.accounts.0c00235.

34. Dreos, A., Börjesson, K., Wang, Z., Roffey, A., Norwood, Z., Kushnir, D., and Moth-Poulsen, K. (2017). Exploring the potential of a hybrid device combining solar water heating and molecular solar thermal energy storage. Energy Environ. Sci. *10*, 728–734. https://doi.org/10.1039/C6EE01952H.

35. Kashyap, V., Sakunkaewkasem, S., Jafari, P., Nazari, M., Eslami, B., Nazifi, S., Irajizad, P., Marquez, M.D., Lee, T.R., and Ghasemi, H. (2019). Full spectrum solar thermal energy harvesting and storage by a molecular and phase-change hybrid material. Joule *3*, 3100–3111. https://doi.org/10.1016/j.joule.2019.11.001.

36. Wu, S., Li, T., Zhang, Z.-Y., Li, T., and Wang, R. (2021). Photoswitchable phase change materials for unconventional thermal energy storage and upgrade. Matter *4*, 3385–3399. https://doi.org/10.1016/j.matt.2021.09.017.

37. Zhang, Z.-Y., He, Y., Wang, Z., Xu, J., Xie, M., Tao, P., Ji, D., Moth-Poulsen, K., and Li, T. (2020). Photochemical phase transitions enable Coharvesting of photon energy and ambient heat for energetic molecular solar thermal batteries that upgrade thermal energy. J. Am. Chem. Soc. *142*, 12256–12264. https://doi.org/10.1021/jacs.0c03748.

38. Philippopoulos, C., Economou, D., Economou, C., and Marangozis, J. (1983). Norbornadiene-quadricyclane system in the photochemical conversion and storage of solar energy. Ind. Eng. Chem. Prod. Res. Dev. *22*, 627–633. https://doi.org/10.1021/i300012a021.

39. Orrego-Hernández, J., Hölzel, H., Quant, M., Wang, Z., and Moth-Poulsen, K. (2021). Scalable Synthesis of Norbornadienes via in situ Cracking of dicyclopentadiene Using Continuous Flow Chemistry. Eur. J. Org. Chem. *2021*, 5337–5342. https://doi.org/10.1002/ejoc.202100795.

40. Jevric, M., Petersen, A.U., Mansø, M., Kumar Singh, S., Wang, Z., Dreos, A., Sumby, C., Nielsen, M.B., Börjesson, K., Erhart, P., and Moth-Poulsen, K.. (2018). Norbornadiene-based photoswitches with exceptional combination of solar spectrum match and long-term energy storage. Chemistry *24*, 12767–12772. https://doi.org/10.1002/chem.201802932.

41. Petersen, A.U., Hofmann, A.I., Fillols, M., Mansø, M., Jevric, M., Wang, Z., Sumby, C.J., Müller, C., and Moth-Poulsen, K. (2019). Solar energy storage by molecular norbornadiene–quadricyclane photoswitches: polymer film devices. Adv. Sci. (Weinh) *6*, 1900367. https://doi.org/10.1002/advs.201900367.

42. Gibert Roca, M. (2022). On improving the efficiency of organic photovoltaic devices: novel strategies. https://ddd.uab.cat/record/265797.

43. Singh, P., Singh, S., Lal, M., and Husain, M. (2008). Temperature dependence of I–V characteristics and performance parameters of silicon solar cell. Sol. Energy Mater. Sol. Cells *92*, 1611–1616. https://doi.org/10.1016/j.solmat.2008.07.010.

44. Singh, P., and Ravindra, N.M. (2012). Temperature dependence of solar cell performance—an analysis. Sol. Energy Mater. Sol. Cells *101*, 36–45. https://doi.org/10.1016/j.solmat.2012.02.019.

45. Fan, J.C.C. (1986). Theoretical temperature dependence of solar cell parameters. Sol. Cells *17*, 309–315. https://doi.org/10.1016/0379-6787(86)90020-7.

46. Lee, T.D., and Ebong, A.U. (2017). A review of thin film solar cell technologies and challenges. Renew. Sustain. Energ. Rev. *70*, 1286–1297. https://doi.org/10.1016/j.rser.2016.12.028.

47. Wang, Z., Losantos, R., Sampedro, D., Morikawa, M.-a., Börjesson, K., Kimizuka, N., and Moth-Poulsen, K. (2019). Demonstration of an azobenzene derivative based solar thermal energy storage system. J. Mater. Chem. A *7*, 15042–15047. https://doi.org/10.1039/C9TA04905C.

48. Aydin, E., Allen, T.G., De Bastiani, M., Razzaq, A., Xu, L., Ugur, E., Liu, J., and De Wolf, S. (2024). Pathways toward commercial perovskite/silicon tandem photovoltaics. Science *383*, eadh3849. https://doi.org/10.1126/science.adh3849.

49. Rühle, S. (2016). Tabulated values of the Shockley–Queisser limit for single junction solar cells. Sol. Energy *130*, 139–147. https://doi.org/10.1016/j.solener.2016.02.015.

50. Liu, D., Yang, C., and Lunt, R.R. (2018). Halide perovskites for selective ultraviolet-harvesting transparent photovoltaics. Joule *2*, 1827–1837. https://doi.org/10.1016/j.joule.2018.06.004.

51. Green, M., Dunlop, E., Hohl-Ebinger, J., Yoshita, M., Kopidakis, N., and Hao, X. (2021). Solar cell efficiency tables (version 57). Prog. Photovolt. *29*, 3–15. https://doi.org/10.1002/pip.3371.

52. The National Renewable Energy Laboratory (2003). Reference air mass 1.5 spectra. https://www.nrel.gov/grid/solar-resource/spectra-am1.5.html.

53. Green, M.A., and Bremner, S.P. (2016). Energy conversion approaches and materials for high-efficiency photovoltaics. Nat. Mater. *16*, 23–34. https://doi.org/10.1038/nmat4676.

54. Waidhas, F., Jevric, M., Fromm, L., Bertram, M., Görling, A., Moth-Poulsen, K., Brummel, O., and Libuda, J. (2019). Electrochemically controlled energy storage in a norbornadiene-based solar fuel with 99% reversibility. Nano Energy *63*, 103872. https://doi.org/10.1016/j.nanoen.2019.103872.

55. Sharma, P.K., Ram, S., and Chandak, N. (2016). Transition metal-free approach to Propynenitriles and 3-Chloropropenenitriles. Adv. Synth. Catal. *358*, 894–899. https://doi.org/10.1002/adsc.201501103.

56. Trost, B.M., Hung, C.-I., and Scharf, M.J. (2018). Direct Catalytic Asymmetric Vinylogous Additions of α,β- and β,γ-butenolides to Polyfluorinated Alkynyl Ketimines. Angew. Chem. Int. Ed. Engl. *57*, 11408–11412. https://doi.org/10.1002/anie.201806249.

57. Hansen, M.H., Olsen, S.T., Sylvester-Hvid, K.O., and Mikkelsen, K.V. (2019). Simulation framework for screening of molecular solar thermal systems in the context of a hybrid device. Chem. Phys. *519*, 92–100. https://doi.org/10.1016/j.chemphys.2018.10.020.